Received: 6 July 2022 | Revised: 15 November 2022 | Accepted: 23 November 2022

DOI: 10.1002/jev2.12291

RESEARCH ARTICLE

Comparison of viral inactivation methods on the characteristics of extracellular vesicles from SARS-CoV-2 infected human lung epithelial cells

Supasek Kongsomros[1,2,3] | **Nutkridta Pongsakul**[2] | **Jirawan Panachan**[4] | **Ladawan Khowawisetsut**[5] | **Jinjuta Somkird**[5] | **Chak Sangma**[6] | **Tapanee Kanjanapruthipong**[7] | **Patompon Wongtrakoongate**[8] | **Arthit Chairoungdua**[8] | **Kovit Pattanapanyasat**[9] | **David S. Newburg**[10] | **Ardythe L. Morrow**[10,11] | **Suradej Hongeng**[4] | **Arunee Thitithanyanont**[3] | **Somchai Chutipongtanate**[1,2,10]

[1]Chakri Naruebodindra Medical Institute, Faculty of Medicine Ramathibodi Hospital, Mahidol University, Samut Prakan, Thailand

[2]Pediatric Translational Research Unit, Department of Pediatrics, Faculty of Medicine Ramathibodi Hospital, Mahidol University, Bangkok, Thailand

[3]Department of Microbiology, Faculty of Science, Mahidol University, Bangkok, Thailand

[4]Division of Hematology and Oncology, Department of Pediatrics, Faculty of Medicine Ramathibodi Hospital, Mahidol University, Bangkok, Thailand

[5]Department of Parasitology, Faculty of Medicine Siriraj Hospital, Mahidol University, Bangkok, Thailand

[6]Department of Chemistry, Faculty of Science, Kasetsart University, Bangkok, Thailand

[7]Department of Tropical pathology, Faculty of Tropical medicine, Mahidol University, Bangkok, Thailand

[8]Department of Biochemistry, Faculty of Science, Mahidol University, Bangkok, Thailand

[9]Center of Excellence for Microparticle and Exosome in Diseases, Research Department, Faculty of Medicine Siriraj Hospital, Mahidol University, Bangkok, Thailand

[10]Division of Epidemiology, Department of Environmental and Public Health Sciences, University of Cincinnati College of Medicine, Cincinnati, Ohio, USA

[11]Division of Infectious Diseases, Department of Pediatrics, Cincinnati Children's Hospital Medical Center, Cincinnati, Ohio, USA

Correspondence
Somchai Chutipongtanate, PhD, MD, Division of Epidemiology, Department of Environmental and Public Health Sciences, University of Cincinnati College of Medicine, 160 Panzeca Way, Cincinnati, OH 45267, USA.
Email: chutipsi@ucmail.uc.edul, schuti.rama@gmail.com

Arunee Thitithanyanont, MD, Department of Microbiology, Faculty of Science, Mahidol University, 272 Rama VI Rd., Ratchathewi, Bangkok 10400, Thailand.
Email: arunee.thi@mahidol.edu

Funding information
Office of National Higher Education Science Research and Innovation Policy Council (PMU-B), Thailand, Grant/Award Numbers: B05F630082, B17F640004, B17F640005; Good Ventures

Abstract

The interaction of SARS-CoV-2 infection with extracellular vesicles (EVs) is of particular interest at the moment. Studying SARS-CoV-2 contaminated-EV isolates in instruments located outside of the biosafety level-3 (BSL-3) environment requires knowing how viral inactivation methods affect the structure and function of extracellular vesicles (EVs). Therefore, three common viral inactivation methods, ultraviolet-C (UVC; 1350 mJ/cm^2), β-propiolactone (BPL; 0.005%), heat (56°C, 45 min) were performed on defined EV particles and their proteins, RNAs, and function. Small EVs were isolated from the supernatant of SARS-CoV-2-infected human lung epithelial Calu-3 cells by stepwise centrifugation, ultrafiltration and qEV size-exclusion chromatography. The EV isolates contained SARS-CoV-2. UVC, BPL and heat completely abolished SARS-CoV-2 infectivity of the contaminated EVs. Particle detection by electron microscopy and nanoparticle tracking was less affected by UVC and BPL than heat treatment. Western blot analysis of EV markers was not affected by any of these three methods. UVC reduced SARS-CoV-2 spike detectability by quantitative RT-PCR and slightly altered EV-derived β-actin detection.

Foundation; National Institute of Allergy and Infectious Diseases, Grant/Award Number: U01AI144673; National Research Council of Thailand, Grant/Award Number: N42A650870

Fibroblast migration-wound healing activity of the SARS-CoV-2 contaminated-EV isolate was only retained after UVC treatment. In conclusion, specific viral inactivation methods are compatible with specific measures in SARS-CoV-2 contaminated-EV isolates. UVC treatment seems preferable for studying functions of EVs released from SARS-CoV-2 infected cells.

KEYWORDS
comparison, COVID-19, exosomes, SARS-CoV-2, small extracellular vesicles, sterilization

1 | INTRODUCTION

Coronavirus disease-19 (COVID-19), caused by the severe acute respiratory syndrome coronavirus 2 (SARS-CoV-2), became a pandemic in March 2020, leading to 525 million confirmed cases and 6.2 million deaths globally as of May 29, 2022 (https://covid19.who.int). Many new variants of SARS-CoV-2 have emerged over time during this pandemic (Karim & Karim, 2021). Continuous efforts have been made to better understand SARS-CoV-2 biology and pathogenesis for developing effective therapeutic strategies and preventive measures against COVID-19. Studies using live SARS-CoV-2 are restricted to being conducted under biosafety level-3 (BSL-3) protocols in a BSL-3 certified laboratory (Centers for Disease Control and Prevention, 2020; Kaufer et al., 2020). Thus, all infected specimens released from the BSL-3 laboratory require an inactivation process to destroy viral infectivity before downstream analyses outside of the BSL-3 laboratory.

Several inactivation methods have been recommended for SARS-CoV-2 (Gupta et al., 2021; Jureka et al., 2020; Loveday et al., 2021; Welch et al., 2020). Chemical methods are commonly used. Detergents such as Triton X-100 and NP-40 inactivate viruses by disrupting the membrane and viral envelope to release internal materials (Welch et al., 2020). Lysis buffer for RNA extraction usually contains guanidinium isothiocyanate, which is known as a general protein denaturant and that can be used to deactivate viruses (Welch et al., 2020). Fixative reagents such as paraformaldehyde and glutaraldehyde lead to the formation of intermolecular cross-links, which are used to inactivate the virus as well as to preserve the virion morphology and antigenicity (Delrue et al., 2012; Jureka et al., 2020; Möller et al., 2015). β-propiolactone (BPL) has also been used to inactivate viruses for vaccine purposes, as it preserves the antigenic properties well (Delrue et al., 2012; Sanders et al., 2015). For physical methods, heat inactivation has been used widely for many viruses as the high temperature denatures thermolabile proteins and other molecules, resulting in impaired molecular functions (Kampf et al., 2020). The use of 56°C for 45 min has been shown to inactivate SARS-CoV-2 completely (Jureka et al., 2020; Loveday et al., 2021). Ultraviolet (UV) irradiation, especially the high-energy UVC (wavelength of 200–280 nm), has been used as an effective method to inactivate viruses, including SARS-CoV-2. UVC irradiation induces SARS-CoV-2 viral genome damage while preserving the structure of virion and integrity of viral proteins (Heilingloh et al., 2020; Lo et al., 2021; Loveday et al., 2021).

Interest in the roles of extracellular vesicles (EVs) during SARS-CoV-2 infection has been growing since EVs and RNA viruses share the cellular vesiculation machinery for biogenesis and release (Gould et al., 2003; Gurunathan et al., 2021; Kongsomros et al., 2021; Nolte et al., 2016; Nunez Lopez et al., 2021). EVs released from the infected cells may modulate immune responses in favour of viral infection, or act as a trojan EV to carry the viral materials transporting between cells to facilitate viral replication (Gould et al., 2003; Gurunathan et al., 2021; Nunez Lopez et al., 2021). The EV inhibitor calpeptin could prevent such infectious virion release and enhance the antiviral effect of remdesivir (Kongsomros et al., 2021). Further investigations of the isolates of small cellular particles from SARS-CoV-2 infected cells would advance our understanding of COVID-19 pathophysiology and may lead to new therapeutic strategies. Nonetheless, there is a safety concern regarding such research as EVs and viruses are presented as a mixed population of nanoscale particles that are not possible to completely separate by current technologies (Nolte et al., 2016; Nunez Lopez et al., 2021). Therefore, the complete viral inactivation of EVs generated from SARS-CoV-2 infected cells is a prerequisite to ensure the safe handling of samples for all experiments outside of the BSL-3 laboratory. Which viral inactivation method is compatible with downstream analyses of particle, protein, RNA, and function of isolated EVs in the context of SARS-CoV-2 infection has not yet been determined.

This study compares the effects of UVC irradiation, BPL, and heat treatment on the characteristics of EVs released from SARS-CoV-2 infected human lung epithelial (Calu-3) cells. Detergents or lysis buffers were used as part of specific experiments but not included into the comparison because they are not compatible with downstream analyses of EV particle and function. After treatment, EV particle, protein and RNA were then evaluated following the International Society for Extracellular Vesicles (ISEV) guidelines (Théry et al., 2018). As little is known about the functions of EVs released from SARS-CoV-2 infected Calu-3 cells, this study preliminarily determined the effects of viral inactivation methods on the known functionality of mesenchymal stem cell-derived extracellular vesicles (MSC-EVs) (Chutipongtanate et al., 2022) following with the specimens containing EVs and virions, by using fibroblast migration-wound healing assay. The entire workflow of this study has been illustrated in Figure 1.

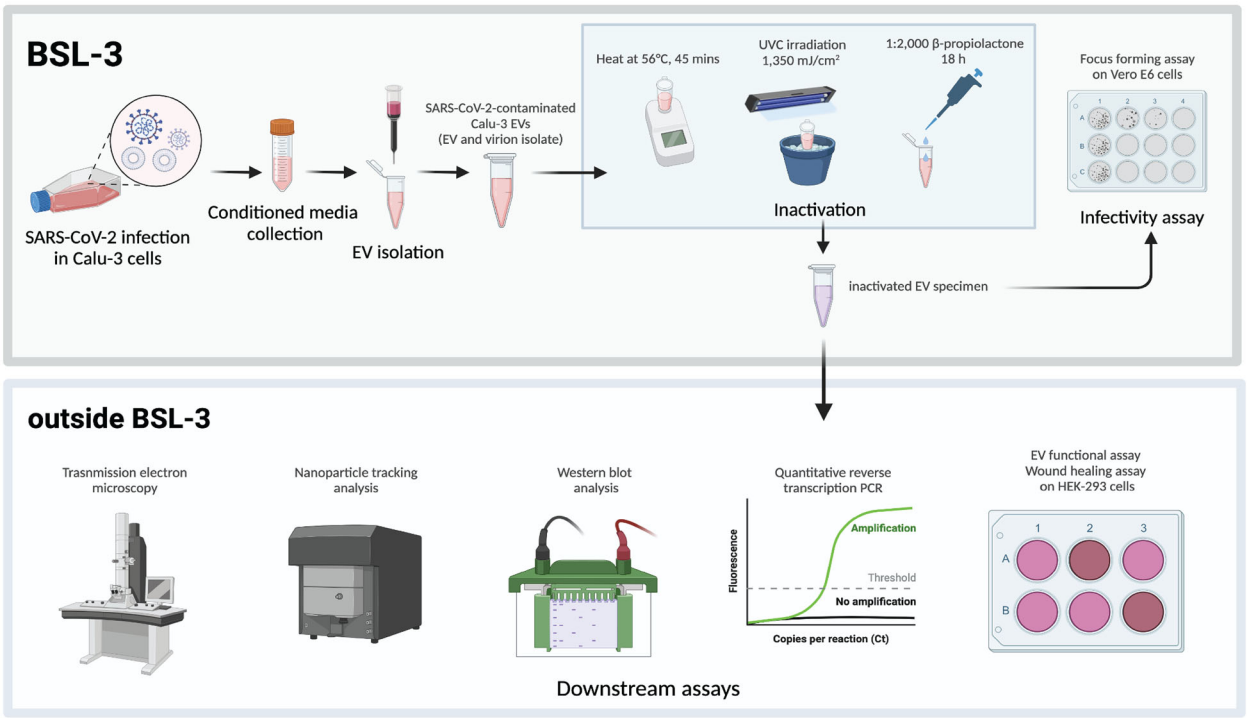

FIGURE 1 Schematic diagram of the experiments conducted inside and outside of the BSL-3 laboratory

In this report, EVs are defined as small EVs or the small subpopulation of extracellular vesicles, and the term "EV and virion isolate" indicates the presence of infectious SARS-CoV-2 viral particles in the EV isolate.

2 | MATERIALS AND METHODS

2.1 | Cell culture

Vero E6 cells, African green monkey (Cercopithecus aethiops) kidney epithelial cells (ATCC®CRL-1586™), were cultured in DMEM (Gibco, NY, USA) with 10% fetal bovine serum (FBS) (Gibco), 100 U/ml penicillin (Gibco), and 100 μg/ml streptomycin (Gibco). The HEK-293 cell line, human embryonic kidney fibroblasts (ATCC®CRL-1573), was cultured in DMEM high glucose supplemented with 10% FBS and 1% penicillin/streptavidin. The Calu-3 cell line, ATCC HTB-55 was cultured in DMEM/F12 with 1% penicillin/streptavidin (Gibco) and supplemented with 10% FBS and 1% GlutaMAX (Gibco). The UC-MSCs, Umbilical cord-derived MSCs (ATCC®PCS-500-010), were purchased from the American Type Culture Collection (ATCC) and were maintained in complete media containing MEM supplemented with 1% L-glutamine, 2% FBS (EVs depleted) and 1% penicillin-streptomycin. The culture medium was replaced every 48 h. All cells were grown at 37°C in a 5% CO_2 water-saturated atmosphere.

2.2 | Virus

SARS-CoV-2 virus (SARS-CoV-2/01/human/Jan2020/Thailand) was isolated from nasopharyngeal swabs of a confirmed COVID-19 patient in Thailand. Nasopharyngeal swab samples in viral transport media (VTM) containing 200 U/ml penicillin, 200 ug/ml streptomycin (Gibco, NY, USA), and 0.25 ug/ml Amphotericin B were centrifuged for 1 min at 10,000 RPM and passed through a sterile 0.45 μm pore size syringe filter. The Vero E6 cell monolayer was used for the virus isolation. The cells were washed once with PBS and then inoculated with undiluted VTM samples, incubated in a CO_2 incubator at 37°C for 2 h, cells were washed with PBS, and the infection media was replaced with 2% FBS in DMEM with 100 U/ml penicillin, and 100 μg/ml streptomycin (Gibco). The infected cells were incubated in a CO_2 incubator at 37°C, and the cytopathic effect (CPE) of the virus on the cells was scored every day. The culture supernatant of the CPE positive was collected and stored at −80°C for the first passage. The virus was propagated in Vero E6 cells by two passages to establish a high-titer stock (passage 3). Viral titers were determined by plaque assay. For SARS-CoV-2 infection in Calu-3 cells, the virus stock was adsorbed onto Calu-3 cells at 37°C for 1 h. SARS-CoV-2 infected Calu-3 cells were washed, and the infection media was replaced with Opti-MEM reduced serum

medium (Gibco) with 100 U/ml penicillin, and 100 μg/ml streptomycin (Gibco), and supplemented with 1% GlutaMAX (Gibco) to reduce the contamination factor of EVs from FBS. Infected cells were incubated at 37°C with 5% CO_2. Virus-containing supernatant was collected on day 3 post-infection for EV isolation. All procedures involving SARS-CoV-2 were performed in a certified BSL-3 laboratory at the Department of Microbiology, Faculty of Science, Mahidol University, Thailand.

2.3 | EV isolation

EV isolation was performed by a combination of step-wise centrifugation, ultrafiltration and qEV size exclusion chromatography, as described previously (Chutipongtanate et al., 2022). SARS-CoV-2 infected Calu-3 supernatant (100 ml; for the EV and virion isolate) or MSC culture media (100 ml; for MSC-EVs) were subjected to step-wise centrifugation at 2000 × *g*, 10 min, and 15,000 x *g*, 60 min. The supernatant was then concentrated by using 100-kDa cutoff centrifugal filtration (Thermo Scientific) to achieve 100 times concentrate (1 ml). The concentrated sample was loaded onto an Izon qEV size-exclusion column (qEVoriginal/35 nm) (Izon Science, UK) to isolate the particles from the soluble protein contaminates. The particle eluates were pooled and concentrated by 10-kDa cutoff centrifugal filtration (Thermo Scientific), resulting in the final volume of 500 μl. All isolation processes were performed at 4°C, or on ice, as appropriate. The isolated EVs were divided into 50 μl aliquots and kept at −80°C until used.

2.4 | Viral inactivation

2.4.1 | UVC

EV and virion isolates (50 μl) in 1.5-ml eppendorf tubes were exposed to UVC radiation using a 254-nm UVC mercury lamp (Sankyo Denki G8T5). The sample was placed on ice at 5 cm below the UVC source, where UVC intensity was 1500 mW/cm^2 measured by a UVC Light Meter (Lutron electronic enterprise Co., Ltd.; model: UVC-254). The sample was irradiated for 15 min, corresponding to the UVC dosage of 1350 mJ/cm^2, before further analysis.

2.4.2 | β-propiolactone (BPL)

Two percent of BPL was added into the EV and virion isolate (50 μl) in a 1.5-ml eppendorf tube to a final concentration of 0.005%. The mixture was incubated at least 18 h at 4°C and then placed in 37°C water bath for 2 h to hydrolyse the residual BPL before further analysis.

2.4.3 | Heat treatment

The EV and virion isolate (50 μL) in a 1.5-ml eppendorf tube was heated at 56°C for 45 min by using a Thermomixer (Eppendorf, Hamburg, Germany). Thereafter, the sample was cooled on ice before further analysis.

2.5 | Transmission electron microscopy

The EV and virion isolates were fixed in 2% glutaraldehyde (AppliChem GmbH, Darmstadt, Germany) at 4°C for 2 h. Five microliters of the fixed sample was applied to a 200 mesh grid (FCF200-CU; Electron Microscopy Sciences) and negatively stained with 2% uranyl acetate (#22400; Electron Microscopy Sciences) in 50% methanol for 1 min, and then dried at room temperature. Imaging was performed using a transmission electron microscope (TEM; HT7700, HITACHI, Japan) with an acceleration voltage of 100 kV at the Faculty of Tropical Medicine, Mahidol University, Bangkok, Thailand.

2.6 | Nanoparticle tracking analysis (NTA)

A NanoSight NS300 (Malvern Instruments Ltd., Malvern, Worcestershire, UK) was used with an integrated sample pump. The sample was diluted 1:10 in PBS to a final volume of 1 ml. The diluted sample was injected into the sample chamber using the syringe pump. Five 1-min videos were captured for each sample with the following parameters; camera: sCMOS; cell temperature: 25°C; syringe pump speed: 30 μl/s. After capture, the videos were analysed by NanoSight Software NTA 3.4 Build

3.4.003 using the settings: detection threshold, 5; blur size and max jump distance, auto. Ideal concentrations contained 20–100 particles/frame.

2.7 | SDS-PAGE and Western blot analysis

The EV sample (20 μg protein) was mixed with 4x Leammli buffer, heated at 95°C for 10 min, and then resolved in the 12% SDS-PAGE before being transferred onto a PVDF membrane using a transblot (Bio-Rad, Hercules, CA, USA). The membrane was blocked with 5% BSA in PBS-T, and then probed with primary antibodies as follows; rabbit anti-Hsp70 (1:1000) (ab79852; Abcam, Waltham, MA, USA), rabbit anti-Tsg101 (1:1000; rabbit), rabbit anti-CD9 (1:1000) (ab223052; Abcam), rabbit anti-CD63 (1:1000) (ab134045; Abcam), or rabbit anti-viral NP (1:1000) (Sino Biological Inc., Beijing, China) antibodies for at 4°C overnight. After washing, the membranes were incubated with goat anti-rabbit IgG-HRP (Dako, Glostrup, Denmark) at room temperature for 1 h. The immunoblot was developed by ECL (Bio-Rad, USA) and imaged on a Bio-Rad Chemidoc imaging system (Bio-Rad, USA). Another SDS-PAGE was performed to visualize total protein bands by Coomassie blue G-250 staining (Bio-Rad, USA).

2.8 | Quantitative RT-PCR

Equal aliquots (50 μL) of EV isolate were transferred into 1.5 ml tubes and subjected to inactivation processes. Then, total RNAs were extracted by miRNeasy plus Mini kits (Qiagen, Hilden, Germany) following the manufacturer's instructions. RT-qPCR assays were performed using QIAGEN OneStep RT-PCR kit (Qiagen, Hilden, Germany), with 4 μl of 5X QIAGEN One step RT-PCR buffer, 0.8 μl of 10 mM nucleotides dNTP mix, 1.2 μl of 10 μM primers, 0.25 μl of SYBR Green, 0.8 μl QIAGEN enzyme mix, 2 μl of RNA template RNA, and 9.75 μl RNase-free water. Ten-fold serial dilutions of SARS-CoV-2 Spike RNA and β-actin plasmid containing 10^7 copies/μl were used for generation of the standard curve to determine the absolute quantity of RNA copies. The following primers were used: β-actin forward (5′-CCA CAC TGT GCC CAT CG-3′); β-actin reverse (5′-AGG ATC TTC ATG AGG TAG TCA GTC AG-3′); Spike forward (5′- CCT ACT AAA TTA AAT GAT CTC TGC TTT ACT-3′); Spike reverse (5′-CAA GCT ATA ACG CAG CCT GTA -3′). Thermal cycling conditions were as follow: 50°C for 30 min, 95°C for 15 min followed by 40 cycles at 95°C for 30 s, 55°C for 30 s and 72°C for 60 s. RT-qPCR assays used the Rotor-Gene Q qPCR system (QIAGEN, Hilden, Germany). Analysis of the copy numbers and linear regression curve were performed using the software Rotor Gene Q (QIAGEN, Germany).

2.9 | Focus forming assay

Direct quantification of infectious virus in inactivated samples and culture supernatant was performed by the focus forming assay in Vero E6 cells. Vero E6 cells were inoculated with ten-fold serially diluted samples in 96-well plates for 1 h. The inoculum was removed, and the cell monolayer was overlaid with 2% FBS in DMEM medium containing 1.2% Avicel (RC581; FMC Biopolymer), then incubated at 37°C in water-saturated 5% CO_2 for 24 h. The cell monolayer was fixed with 4% formaldehyde in PBS for 1 h, and then washed three times with PBS. To detect the viral foci, cells were permeabilized in 0.5% triton X-100 at room temperature for 10 min, then washed with PBS twice, and incubated with 1:2,500 rabbit monoclonal antibody against SARS-CoV-2 Nucleoprotein (Sino Biological Inc., China) at room temperature for 1 h. Cells were then washed with PBS thrice, followed by incubation with 1:1000 horseradish peroxidase-conjugated goat anti-rabbit IgG secondary antibody (DAKO, CA, USA) and stained with True-Blue peroxidase substrate (Sera Care, Milford, MA, USA). Viral foci were counted and calculated as focus forming units (FFU) per ml.

2.10 | Wound healing assay

HEK-293 cells were seeded into a 96-well plate (3×10^5 cells/well). The scratch wound was performed with a 10 μl pipette tip. Cells were washed once with the culture media to remove the detached cells. Fresh culture media containing MSC-EVs or SARS-CoV-2-contaminated Calu-3 EVs, before (native) or after inactivation procedures, at the concentration of 1,000 particles per cell were added. The blank condition (only culture media) and IGF (100 ng) treatment were included as the negative and positive controls, respectively. The area of the scratched wound was measured at 0 and 24 h at 4× magnification under an inverted microscope (Motic AE2000; Kowloon, Hong Kong). Quantification of wound closure was determined using ImageJ software (National Institutes of Health, Bethesda, MD, USA). Results are presented as percentage of wound closure at 24 h. All data values in this experiment represent three biological replicates.

2.11 | Statistical analysis

All statistical tests were performed using GraphPad Prism 7 (GraphPad Company, San Diego, CA, USA). One-way analysis of variance (ANOVA) was used to compare differences among groups. P-value < 0.05 was considered statistically significant.

3 | RESULTS

3.1 | Isolation and validation of EVs released from SARS-CoV-2-infected Calu-3 cells

Calu-3 cells were infected with SARS-CoV-2 at the multiplicity of infection (moi) of 0.05 for 48 h. EVs released in the supernatant of SARS-CoV-2 infected and uninfected Calu-3 cells were isolated by a combination of step-wise centrifugation, ultrafiltration and qEV size exclusion chromatography. Validation of particle and protein evidence confirming the EV presence in the isolate were performed according to the ISEV guideline (Théry et al., 2018), with an extension of viral evidence. In this experiment, 2.5% glutaraldehyde fixation was applied to the EV isolate for particle analysis. The lysis buffers RIPA and miRNAeasy plus mini kit were used to extract EV proteins and RNAs for Western blot and RT-qPCR experiments, respectively.

TEM with negative staining showed EVs as cup-shaped vesicles from both infected and uninfected Calu-3 cells (Figure 2A). Infected and uninfected groups showed similar particle distribution (118.3 ± 1.8 nm vs. 125.7 ± 2.4 nm in diameter) and particle concentration (8.6×10^8 particle/ml vs. 8.9×10^8 particle/ml) by NTA (Figure 2B). EV markers Tsg101, CD63 and CD9 were enriched in EVs compared to cells, as measured by Western blots, while SARS-CoV-2 nucleoprotein was only detected in the EV and virion isolates and infected cell specimens (Figure 2C). RT-qPCR of spike gene confirmed the presence of SARS-CoV-2 in the EV and virion isolate as well as the infected cells (Figure 2D, E). Infectious viral particles were also detected in the EV and virion isolates by the focus forming assay, in which viral particles were more enriched than in the culture medium of infected cells (Figure 2F). These results confirm that the EV isolate contains SARS-CoV-2, and therefore EV isolates require effective and compatible viral inactivation prior to transfer from the BSL-3 laboratory for downstream molecular and functional analyses.

3.2 | UVC radiation, BPL, and heat treatment can completely inactivate SARS-CoV-2

The efficacy of three viral inactivation methods was first validated by using the SARS-CoV-2 viral stock (Figure 3A, B), following by the EV and virion isolates (Figure 3C, D). UVC irradiation, BPL, and heat treatment were performed following standard published protocols (Jureka et al., 2020; Loveday et al., 2021). Each aliquot of 1.5 ml viral stock containing infectious SARS-CoV-2 at 1×10^5 FFU/ml was treated with UVC radiation for 30 min, 1:2,000 BPL overnight, or heat treatment at 56°C for 45 mins (Jureka et al., 2020; Loveday et al., 2021) before assessing the viral infectivity by the focus forming assay. UVC irradiation, BPL, or heat treatment completely inactivated infectivity of the viral stock (Figure 3A, B). When the EV and virion isolates were subjected to these inactivation conditions, no infectious foci were detected in any of the treated specimens (Figure 3C, D). Thus, UVC irradiation, BPL, or heat treatment absolutely inactivated SARS-CoV-2 in the EV and virion isolates, rendering them safe for work outside the BSL-3 environment.

3.3 | UVC radiation and BPL did not affect EV morphology, particle diameter or concentration, but heat treatment did

Whether the inactivation methods altered EV particle characteristics was evaluated by TEM and NTA. TEM images of EVs, which generally appeared as cup-shaped vesicles, were not altered by UVC radiation, BPL, or heat treatment relative to the 2.5% glutaraldehyde fixation controls (Figure 4A). However, heat treatment may have caused a slight vesicle enlargement. UVC and BPL had no effect on the particle size distribution, as measured by NTA, but heat treatment caused a significant vesicle enlargement relative to the glutaraldehyde fixation controls (Figure 4B, C). None of these three inactivation methods changed EV concentrations (Figure 4D). Thus, EV morphology and concentration were maintained after UVC irradiation, BPL or heat treatment, but heat inactivation enlarged EV diameters.

3.4 | Neither UVC radiation, BPL, nor heat treatment affected detectable EV proteins

To determine whether viral inactivation allowed EV and viral proteins in the EV and virion isolates to remain intact and still react with antibodies, Western blot analysis was performed using antibodies against the EV markers HSP70, Tsg101, and CD9,

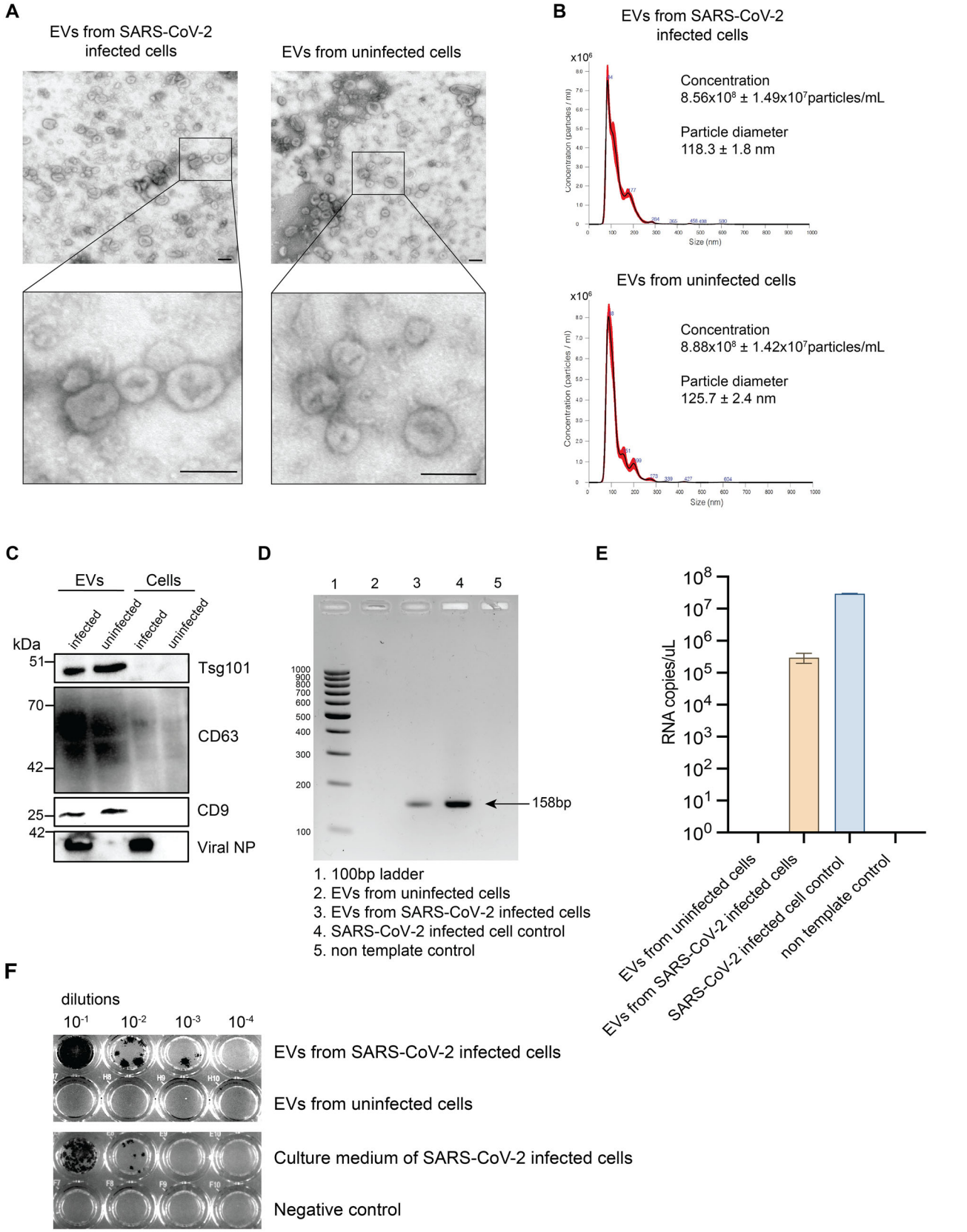

FIGURE 2 EVs and SARS-CoV-2 co-exist in the EV and virion isolate. (A) Transmission electron microscopy shows a cup-shape morphology of EVs isolated from SARS-CoV-2 infected and uninfected Calu-3 human lung epithelial cells. Scale bar, 100 nm. (**B**) Size distribution of EVs was determined by NTA. The particle concentration and diameter are presented as the mean ± SD. (**C**) Presence of EV markers (i.e., CD63, CD9 and Tsg101) and SARS-CoV-2 nucleoprotein (NP) detected by Western immunoblot (the full-length blot images were available in Supplementary figure 1). Total RNAs were extracted from the EV and virion isolates and infected cells. RT-qPCR was performed using primers specific to the SARS-CoV-2 spike. (**D**) Ethidium bromide stained gel

(Continues)

FIGURE 2 (Continued)
shows the presence of amplified SARS-CoV-2 products in the EV and virion isolates and infected cell samples. (**E**) The copy number of the SARS-CoV-2 spike gene was determined by RT-qPCR. Viral infectivity of isolated EVs from SARS-CoV-2 infected- and uninfected-cells was compared by the focus forming assay. (**F**) Representative images of the SARS-CoV-2 foci observed in the EV and virion isolates from SARS-CoV-2 infected Calu-3 cells. Negative control was the culture medium of uninfected Calu-3 cells

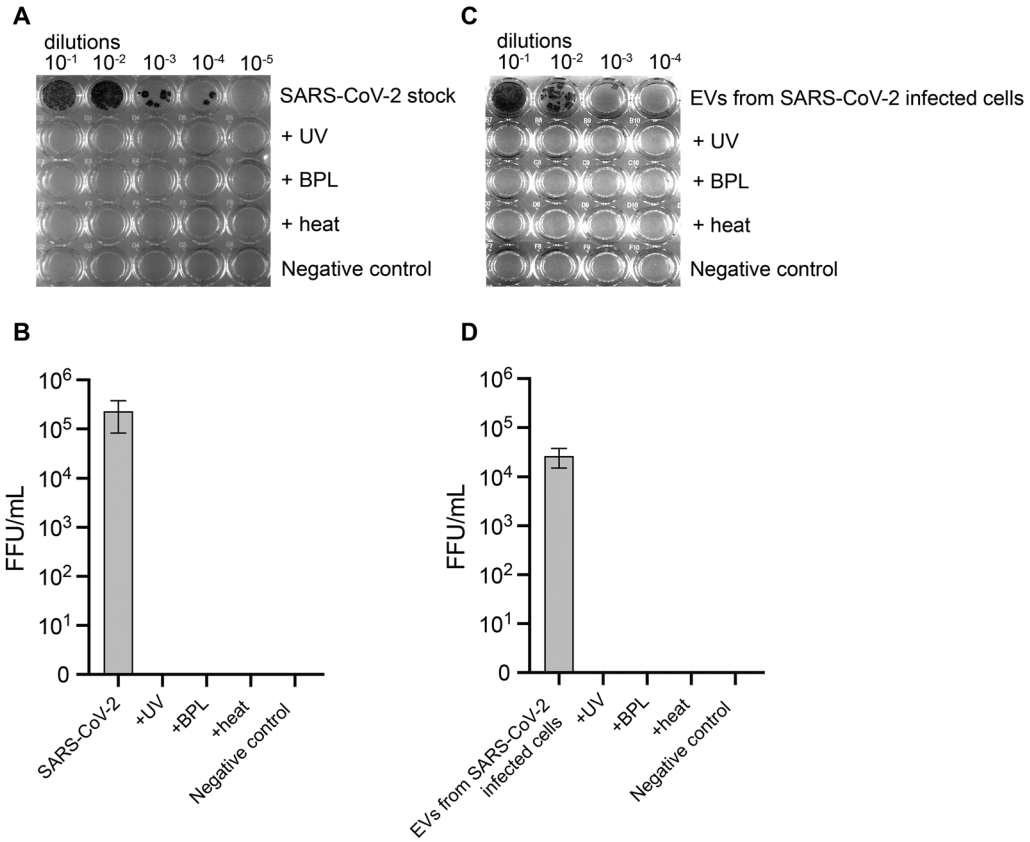

FIGURE 3 SARS-CoV-2 infectivity of viral stock and the EV and virion isolate after UVC irradiation, BPL, or heat treatment. SARS-CoV-2 viral stock at 10^5 FFU/ml was treated with UVC, BPL or heat before measuring the number of infectious virions by the focus forming assay (FFA). The viral titers in focus forming units (FFU) were calculated. No SARS-CoV-2 foci of viral stock were detected following each of viral inactivation methods (**A, B**). After the EV and virion isolates were inactivated by UVC, BPL or heat treatment, no detectable infectious SARS-CoV-2 foci remained (**C, D**). Data are mean ± SD of three biological replicates. Negative control was the culture medium of uninfected Calu-3 cells

and viral NP. Neither UVC, BPL nor heat affected the detectability of these EV markers or viral NP by Western blot analysis (Figure 5). SDS-PAGE with Coomassie blue G-250 staining produced the same protein patterns among the EV samples with or without inactivation processes (Figure 5). Overall protein expression profiles of EVs being indistinguishable by viral inactivation processes suggests that the validated inactivation methods are all suitable for the study of EV protein expressional profiles from SARS-CoV-2 infected Calu-3 cells.

3.5 | 5. SARS-CoV-2 Spike gene copy numbers and EV-derived mRNA levels are reduced by UVC irradiation, somewhat reduced by BPL, but not by heat

The effects of viral inactivation methods were compared on detectable RNA. After UVC irradiation, BPL, or heat treatment, total RNA was extracted from EVs, and SARS-CoV-2 spike gene copy numbers and β-actin mRNA were measured by RT-qPCR. β-actin mRNA is commonly detectable in EVs (Haque & Vaiselbuh, 2018). Figure 6A showed that UVC irradiation, but not heat treatment, decreased the viral RNA copy numbers over 3 orders of magnitude compared to the control condition (EVs subjected directly to the lysis buffer). BPL reduced viral RNA copy numbers only slightly. Figure 6B demonstrated that UVC irradiation also altered the number of β-actin mRNA copies (2.5×10^3 copies) compared to the control condition (1×10^4 copies) (Figure 6B). BPL reduced β-actin mRNA copy numbers only slightly, and heat not at all. In summary, UVC inactivation reduced the amount

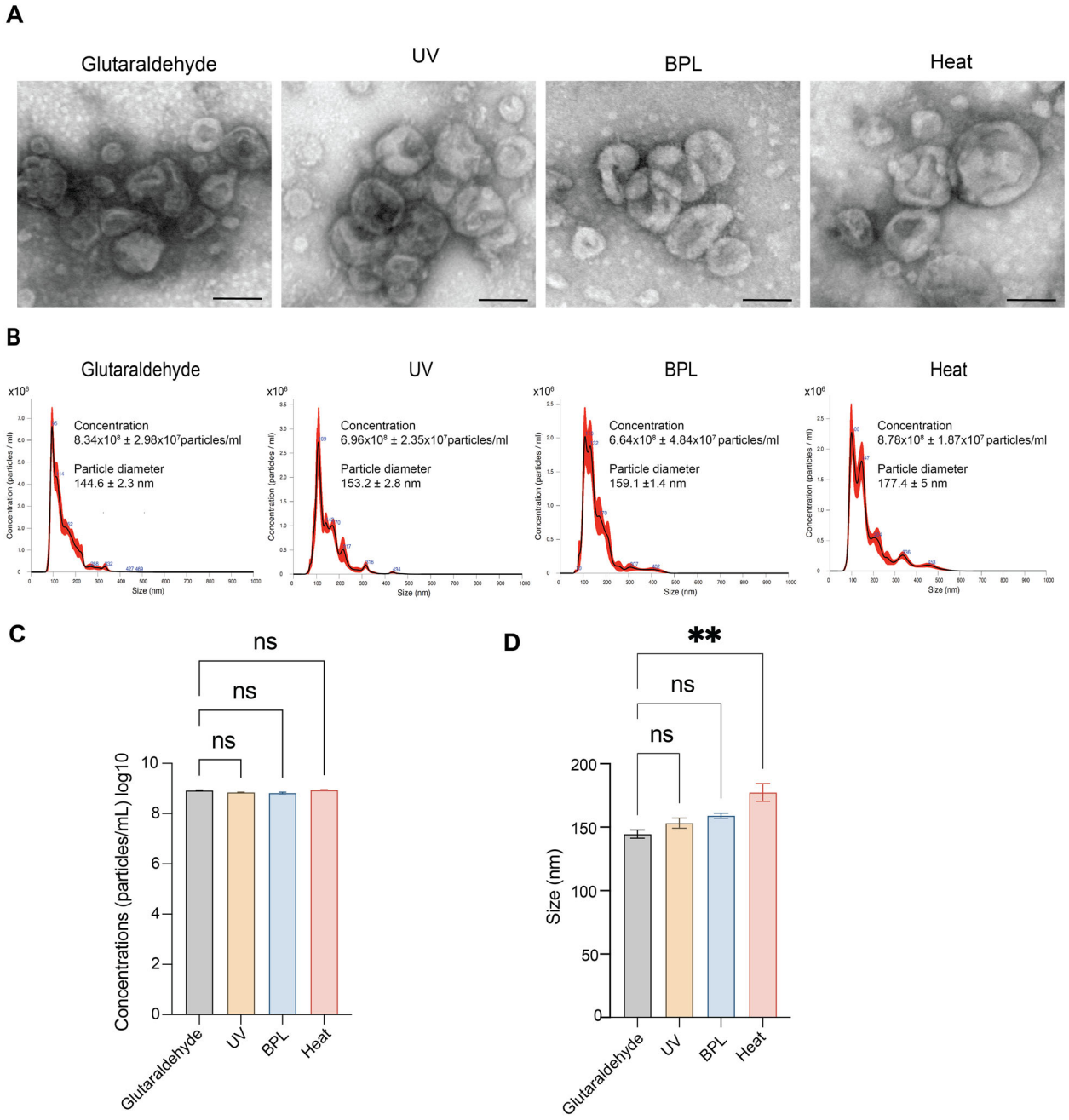

FIGURE 4 EV morphology, particle diameter and concentration of the EV and virion isolates after UVC radiation, BPL, or heat treatment. Fifty microliters of the EV and virion isolates in a 1.5 ml eppendorf tube were exposed to UVC radiation, BPL or heat treatment. (**A**) TEM images of isolated EVs after inactivation are shown. Scale bar, 100 nm. (**B**) NTA showed the size distribution, (**C**) the average diameter, and (**D**) concentration (particles/ml) of the EV and virion isolates after inactivation. Samples fixed in 2.5% glutaraldehyde were negative controls. The data are presented as the mean ± SD of two independent experiments. ns, not significant; **, $p < 0.01$

of RNA detected by RT-qPCR from both viruses and EVs, BPL had only a minor effect, and heat inactivation caused no change in either viral RNA or β-actin mRNA copy numbers.

3.6 | UVC irradiation, but not BPL and heat treatment, preserved MSC-EV wound healing activity

As the biological functions of EVs released from SARS-CoV-2 infected Calu-3 cells are not yet defined, mesenchymal stem cell-derived extracellular vesicles (MSC-EVs) were preliminarily used as a surrogate to examine the effect of viral inactivation processes on EV functionality. MSC-EVs have tissue regeneration and wound healing activity (Casado-Díaz, Quesada-Gómez, &

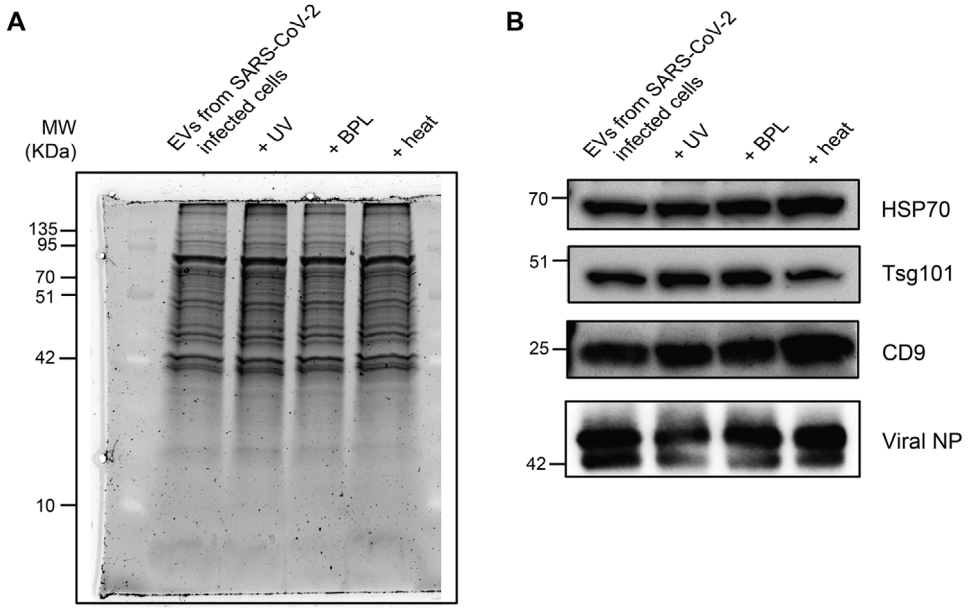

FIGURE 5 SARS-CoV-2 nucleoprotein and EV proteins of the EV and virion isolates after viral inactivation processes. Specimens containing EVs and inactivated virions (20 μg protein each) were lysed by Leammli buffer and separated by 12% SDS-PAGE to analyze (**A**) the protein band patterns by Coomassie Blue-G250 staining or (**B**) subjected to Western immunoblotting to detect EV markers, i.e., Hsp70, Tsg101, CD9, and viral nucleoprotein (NP). The uncropped immunoblot images are in Supplementary figure 2

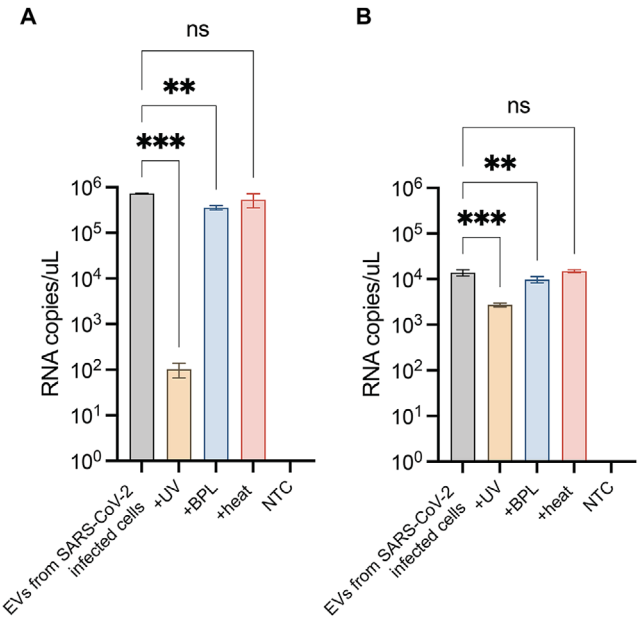

FIGURE 6 **SARS-CoV-2 spike and EV-derived β-actin mRNAs of the EV and virion isolates after inactivation**. Total RNAs were extracted from the specimen containing EVs and inactivated virions. Viral and EV RNA from each inactivation method were assessed by absolute copy number quantification using RT-qPCR targeting spike and β-actin genes. The amount of RNA is demonstrated as the copy number for SARS-CoV-2 spike gene (**A**) and β-actin mRNA (**B**). The data are presented as the mean $\pm$ SD of three biological replicates. NTC, non-template control; ns, not significant; **, $p < 0.01$; ***, $p < 0.001$

Dorado, 2020; Hade, Suire, & Suo, 2021). The scratch wound healing assay measures the regenerative processes of MSC-EVs (Xie et al., 2017). To evaluate the effect of UVC irradiation, BPL, and heat treatments on MSC-EVs functions, we isolated EVs from the MSC culture media as previously described (Chutipongtanate et al., 2022) and then treated them with UVC irradiation, BPL or heat treatment. MSC-EV isolation and validation are shown in Supplementary figure 3. The In vitro scratch wound healing assay determined MSC-EV function after inactivation. UVC irradiation, but not BPL or heat treatment, preserved the wound

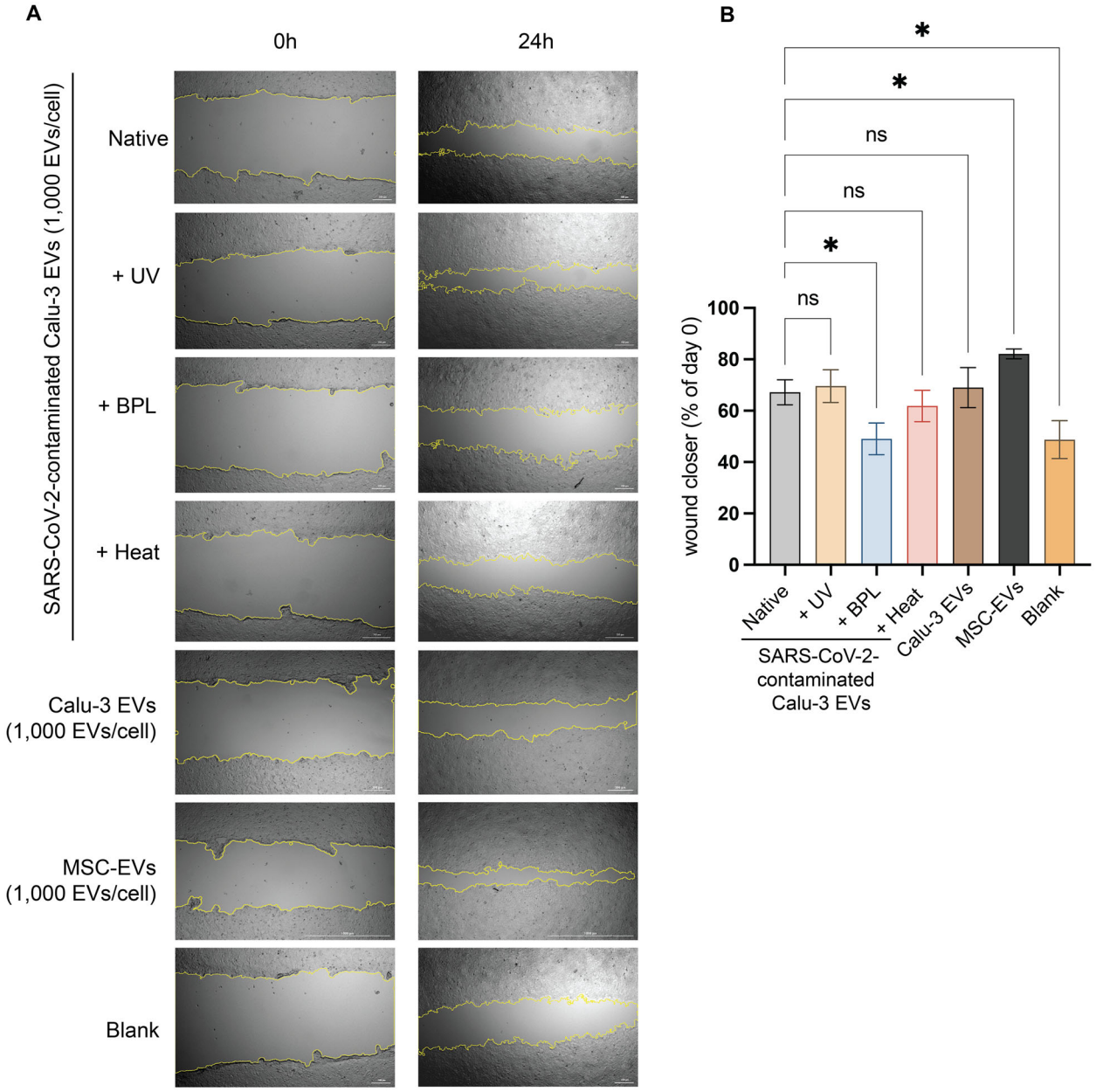

FIGURE 7 Wound healing by the EV and virion isolates after UVC irradiation, BPL, and heat treatment. The *in* vitro wound healing assay of EVs isolated from SARS-CoV-2 infected Calu-3 was performed on a confluent HEK-293 monolayer. The wound was scratched on the cell monolayer by a 200 μl pipette tip followed by treatment with the EV and virion isolates (1000 EVs/cell). (**A**) Representative images of scratches at 0 and 24 h. (**B**) The percentage of wound closure was calculated. Native indicates the EV and virion isolate without the application of viral inactivation. Mesenchymal stem cell-derived extracellular vesicles (MSC-EVs; 1,000 EVs/cell) served as the positive control. The blank condition was the culture media only. The data are presented as the mean ± SD of three biological replicates. ns, not significant; *, $p < 0.05$

healing capability of MSC-EVs comparable to native MSC-EVs (Supplementary figure 4). This preliminary data provided direct evidence of viral inactivation methods on EV functionality without contributions from viral factors.

Promoting tissue development is one of the general EV functions (Cheng & Hill, 2022). We then sorted out whether Calu-3 EVs could enhance fibroblast migration using wound healing-scratch assay. The result showed that Calu-3 EVs, at various dosages of 100 EVs/cell, 1000 EVs/cell and 10,000 EVs/cell, exhibit wound healing capability in a dose-dependent manner (Supplementary figure 5), although having a lower potency than MSC-EVs (at 1000 EVs/cell). This defined function of Calu-3 EVs allowed us to determine the effect of viral inactivation methods on the EV and virion isolates from SARS-CoV-2 infected Calu-3 cells. Figure 7 showed UVC irradiation, but not BPL or heat treatment, preserved wound healing capability of the EV and virion isolates comparable to the native condition (the EV and virion isolate without viral inactivation applied) and Calu-3 EVs

TABLE 1 Comparison of viral inactivation methods on particle, protein, RNA, and function of EVs from SARS-CoV-2 infected sources

	Viral inactivation method		
Downstream analysis	**UVC**	**PBL**	**Heat treatment**
Particle evidence			
TEM morphology	++	++	++
NTA size distribution	++	++	+/–
NTA concentration	++	++	++
Protein integrity *(Western immunoblot)*			
SARS-CoV-2 nucleoprotein	++	++	++
EV markers (CD9, Tsg101, HSP70)	++	++	++
RNA preservation *(RT-qPCR)*			
SARS-CoV-2 spike RNA	+/–	++	++
EV β-actin mRNA	+	++	++
Biological function			
Fibroblast migration (wound healing)	++	–	+/–

Abbreviations: NTA, nanoparticle tracking analysis; TEM, transmission electron microscopy.
++Highly compatible
+Compatible.
+/–May be useful in some situations
–Do not recommend

(no virus). Note that this experiment was performed in the BSL-3 environment due to the use of the specimen containing infectious virions.

Hence, the biological function of MSC-EVs and the Calu-3 EV and virion isolates were not affected by UV inactivation, were slightly decreased by heat treatment, and were very much abrogated by BPL inactivation.

4 | DISCUSSION

EVs play several critical roles during infections. They can carry infectious virion or viral materials to other naïve cells, thereby facilitating viral infection (Caobi et al., 2020). EVs have also been found to carry host components, such as molecules that modulate immune responses. Such findings increase interest in characterizing EVs from infected cells and determining their possible implications for managing SARS-CoV-2 infection (Gurunathan et al., 2021; Nunez Lopez et al., 2021). However, the safety requirements for SARS-CoV-2 related research limit most experiments to the BSL-3 setting. Complete viral inactivation is necessary for transferring the samples from BSL-3 to a lower biosafety level where sophisticated and specialized analysis can be performed while continuing to prevent the possibility of laboratory-acquired infections.

The data herein confirm that the EV samples isolated from SARS-CoV-2 infected Calu-3 supernatant are contaminated with the virus (Figure 2). They further demonstrate that well-established viral inactivation methods are capable of fully inactivating the SARS-CoV-2 contaminant. Three commonly used inactivation methods were compared for their effects on the morphology, integrity of protein and RNA, and functions of isolated EVs. UVC irradiation at a dose of 1350 mJ/cm^2 for 15 min, 0.005% BPL treatment overnight, and heat treatment at 56°C for 45 min completely inactivated SARS-CoV-2 infectivity (Figure 3), consistent with previous studies (Batéjat et al., 2021; Gupta et al., 2021; Jureka et al., 2020; Loveday et al., 2021; Patterson et al., 2020; Welch et al., 2020). None of the inactivation methods disrupted the typical vesicular morphology of the EVs (Figure 4A), but heat-treated EVs had slightly increased particle size not seen in EVs treated with the other methods (Figure 4C). Western blot analysis revealed that the overall detectability of viral NP and EV proteins was not affected by any of the inactivation methods (Figure 5). UVC light can cause the formation of dimers in nucleic acids and induce viral genome degradation (Bono et al., 2021; Lo et al., 2021). As in other studies, the data herein confirm that UVC inactivation reduced the amount of RNA detected by RT-qPCR of both viral and EV origin (Figure 6A, B) (Bono et al., 2021; Lo et al., 2021; Loveday et al., 2021). The effect of UVC inactivation on microRNA (miRNA) cargo in EVs remains of interest as miRNA cargo may to play an important role in the regulation of gene expression in recipient cells (Yang et al., 2016). Evidence of functions by EVs released from SARS-CoV-2 infected Calu-3 cells is sparse; therefore, MSC-EVs (no virus) were used as surrogates to investigate EV function after inactivation processes (Supplementary figure 4), followed by defining a biological function for Calu-3 EVs (no virus) by wound healing-scratch assay (Supplementary figure 5). Those preliminary data supported us in conducting an experiment to determine the effect of viral inactivation methods on the EV and virion isolates (Figure 7). To this end, wound healing efficiency of MSC-EVs (no virus) and the EV and virion isolates were not affected by UV inactivation, was slightly decreased by heat inactivation, and was dramatically abrogated by BPL-inactivation (Supplementary figure 4 and Figure 7). These findings are consistent with the BPL inactivation of influenza virus that is commonly used for the inactivation of influenza virus for vaccines as it preserves antigenicity. However,

BPL-inactivation causes a loss of hemagglutinin (HA) and neuraminidase (NA) function, as well as fusion ability (Bonnafous et al., 2014; Herrera-Rodriguez et al., 2019). Hence, BPL inactivation might not an ideal choice as a viral inactivating reagent for protein functional studies.

This study had limitations. First, this study focused on the physical/chemical methods for viral inactivation. Alternative strategies based on the biological methods, that is, applying neutralizing antibodies for viral inactivation of the EV and virion isolates, or purifying EVs from the isolates containing viruses by antibody capture beads, or a combination of both, warrant further investigations. Second, EVs from specific cell sources may modulate SARS-CoV-2 infectivity, for example, MSCs (Chutipongtanate et al., 2022) and ACE2-expressing cells (Cocozza et al., 2020; El-Shennawy et al., 2022; Tey et al., 2022). Calu-3 cells used in this study are known to express surface ACE2 (Puray-Chavez et al., 2021). Thus, ACE2-expressing EVs derived from Calu-3 cells may prevent SARS-CoV-2 infection via ACE2-spike interaction (Cocozza et al., 2020; El-Shennawy et al., 2022), or vice versa, these ACE2-expressing EVs may facilitate the entry of SARS-CoV-2 into host cells through cellular EV uptake mechanisms (Tey et al., 2022). The dilemma of ACE2-expressing respiratory epithelial cells as the host cell target, and the mechanisms to modulate SARS-CoV-2 infectivity via released ACE2-expressing EVs, should be investigated in future studies.

Little is known about EVs derived from SARS-CoV-2 infected cells with regard to molecular alterations that could enhance or suppress SARS-CoV-2 infectivity of recipient cells. Such information could provide a valuable tool in studying the role of EVs in cell-to-cell communication during SARS-CoV-2 infection. The data from this study should facilitate downstream analysis of EVs from SARS-CoV-2 infected samples with regard to which inactivation methods are compatible with specific types of downstream EV analyses, including morphology, protein, RNA, and function (Table 1). UVC irradiation would be the method of choice in most situations due to its simplicity, accessibility, low cost, and importantly, its preservation of EV function. In particular, UVC irradiation may be the best choice in research involving functions of EVs released from SARS-CoV-2 infected cells.

AUTHOR CONTRIBUTION

Conceptualization, S.C.; methodology, S.K., N.K., J.P., L.K., K.P., A.T., S.C.; validation, P.W., A.C., K.P., S.H., A.T., S.C.; formal analysis, S.K., N.K., J.P., L.K., J.S., C.S., T.K.; investigation, S.K., N.K., J.P., L.K., J.S., C.S., T.K.; resources, P.W., A.C., K.P., D.S.N., A.L.M., S.H., A.T., S.C.; writing—original draft preparation, S.K.; writing—review and editing, N.K., J.P., L.K., J.S., C.S., T.K., P.W., A.C., K.P., D.S.N., A.L.M., S.H., A.T., S.C.; visualization, S.K., N.K., J.P., L.K., T.K., S.C.; supervision, K.P., D.S.N., A.L.M., S.H., A.T., S.C.; funding acquisition, A.T., K.P., A.L.M., S.C. All authors have read and agreed to the published version of the manuscript.

ACKNOWLEDGEMENTS

This study was supported by the Office of National Higher Education Science Research and Innovation Policy Council (PMU-B), Thailand, grant number B17F640004 (S.C.), B05F630082 (S.C.) and B17F640005 (A.T.). K.P. was supported by the National Research Council of Thailand (NRCT)/NSTDA: High-Potential Research Team Grant Program, grant number N42A650870. S.C. and A.L.M. were also supported by the Good Ventures Foundation and NIH/NIAID grant number U01AI144673.

CONFLICTS OF INTEREST

All authors declare no conflicts of interest.

REFERENCES

Batéjat, C., Grassin, Q., & Manuguerra, J.-C. (2021). Heat inactivation of the severe acute respiratory syndrome coronavirus 2. *Journal of Biosafety and Biosecurity*, *3*(1), 1–3.

Bonnafous, P., Nicolaï, M.-C., Taveau, J.-C., Chevalier, M., Barrière, F., Medina, J., Le Bihan, O., Adam, O., Ronzon, F., & Lambert, O. (2014). Treatment of influenza virus with beta-propiolactone alters viral membrane fusion. *Biochimica et Biophysica Acta (BBA)-Biomembranes*, *1838*(1), 355–363.

Bono, N., Ponti, F., Punta, C., & Candiani, G. (2021). Effect of UV irradiation and TiO_2-photocatalysis on airborne bacteria and viruses: An overview. *Materials*, *14*(5), 1075.

Caobi, A., Nair, M., & Raymond, A. D. (2020). Extracellular vesicles in the pathogenesis of viral infections in humans. *Viruses*, *12*(10), 1200.

Casado-Díaz, A., Quesada-Gómez, J. M., & Dorado, G. (2020). Extracellular vesicles derived from mesenchymal stem cells (MSC) in regenerative medicine: Applications in skin wound healing. *Frontiers in Bioengineering and Biotechnology*, *8*, 146.

Centers for Disease Control and Prevention. (2020). (2020). Interim laboratory biosafety guidelines for handling and processing specimens associated with coronavirus disease 2019 (COVID-19). Retrieved from https://stacks.cdc.gov/view/cdc/86282

Cheng, L., & Hill, A. F. (2022). Therapeutically harnessing extracellular vesicles. *Nature Reviews Drug Discovery*, *21*(5), 379–399. https://doi.org/10.1038/s41573-022-00410-w

Chutipongtanate, S., Kongsomros, S., Pongsakul, N., Panachan, J., Khowawisetsut, L., Pattanapanyasat, K., Hongeng, S., & Thitithanyanont, A. (2022). Anti-SARS-CoV-2 effect of extracellular vesicles released from mesenchymal stem cells. *Journal of Extracellular Vesicles*, *11*(3), e12201.

Cocozza, F., Névo, N., Piovesana, E., Lahaye, X., Buchrieser, J., Schwartz, O., Manel, N., Tkach, M., Théry, C., & Martin-Jaular, L. (2020). Extracellular vesicles containing ACE2 efficiently prevent infection by SARS-CoV-2 Spike protein-containing virus. *Journal of Extracellular Vesicles*, *10*(2), e12050. https://doi.org/10.1002/jev2.12050

Delrue, I., Verzele, D., Madder, A., & Nauwynck, H. J. (2012). Inactivated virus vaccines from chemistry to prophylaxis: merits, risks and challenges. *Expert Review of Vaccines*, *11*(6), 695–719.

El-Shennawy, L., Hoffmann, A. D., Dashzeveg, N. K., McAndrews, K. M., Mehl, P. J., Cornish, D., Yu, Z., Tokars, V. L., Nicolaescu, V., Tomatsidou, A., Mao, C., Felicelli, C. J., Tsai, C. F., Ostiguin, C., Jia, Y., Li, L., Furlong, K., Wysocki, J., Luo, X., … Liu, H. (2022). Circulating ACE2-expressing extracellular vesicles block broad strains of SARS-CoV-2. *Nature Communications*, *13*(1), 405. https://doi.org/10.1038/s41467-021-27893-2

Gould, S. J., Booth, A. M., & Hildreth, J. E. (2003). The Trojan exosome hypothesis. *Proceedings of the National Academy of Sciences*, *100*(19), 10592–10597.

Gupta, D., Parthasarathy, H., Sah, V., Tandel, D., Vedagiri, D., Reddy, S., & Harshan, K. H. (2021). Inactivation of SARS-CoV-2 by β-propiolactone causes aggregation of viral particles and loss of antigenic potential. *Virus Research*, *305*, 198555. https://doi.org/10.1016/j.virusres.2021.198555

Gurunathan, S., Kang, M. H., & Kim, J.-H. (2021). Diverse effects of exosomes on COVID-19: A perspective of progress from transmission to therapeutic developments. *Frontiers in Immunology*, *12*, 716407.

Hade, M. D., Suire, C. N., & Suo, Z. (2021). Mesenchymal stem cell-derived exosomes: Applications in regenerative medicine. *Cells*, *10*(8), 1959.

Haque, S., & Vaiselbuh, S. R. (2018). Exosomes molecular diagnostics: Direct conversion of exosomes into the cDNA for gene amplification by two-step polymerase chain reaction. *Journal of Biological Methods*, *5*(3), e96.

Heilingloh, C. S., Aufderhorst, U. W., Schipper, L., Dittmer, U., Witzke, O., Yang, D., Zheng, X., Sutter, K., Trilling, M., Alt, M., Steinmann, E., & Krawczyk, A. (2020). Susceptibility of SARS-CoV-2 to UV irradiation. *American Journal of Infection Control*, *48*(10), 1273–1275. https://doi.org/10.1016/j.ajic.2020.07.031

Herrera-Rodriguez, J., Signorazzi, A., Holtrop, M., de Vries-Idema, J., & Huckriede, A. (2019). Inactivated or damaged? Comparing the effect of inactivation methods on influenza virions to optimize vaccine production. *Vaccine*, *37*(12), 1630–1637. https://doi.org/10.1016/j.vaccine.2019.01.086

Jureka, A. S., Silvas, J. A., & Basler, C. F. (2020). Propagation, inactivation, and safety testing of SARS-CoV-2. *Viruses*, *12*(6), 622.

Kampf, G., Voss, A., & Scheithauer, S. (2020). Inactivation of coronaviruses by heat. *Journal of Hospital Infection*, *105*(2), 348–349.

Karim, S. S. A., & Karim, Q. A. (2021). Omicron SARS-CoV-2 variant: a new chapter in the COVID-19 pandemic. *The Lancet*, *398*(10317), 2126–2128.

Kaufer, A. M., Theis, T., Lau, K. A., Gray, J. L., & Rawlinson, W. D. (2020). Laboratory biosafety measures involving SARS-CoV-2 and the classification as a Risk Group 3 biological agent. *Pathology*, *52*(7), 790–795. https://doi.org/10.1016/j.pathol.2020.09.006

Kongsomros, S., Suksatu, A., Kanjanasirirat, P., Manopwisedjaroen, S., Prasongtanakij, S., Jearawuttanakul, K., Borwornpinyo, S., Hongeng, S., Thitithanyanont, A., & Chutipongtanate, S. (2021). Anti-SARS-CoV-2 activity of extracellular vesicle inhibitors: Screening, validation, and combination with remdesivir. *Biomedicines*, *9*(9), 1230.

Lo, C.-W., Matsuura, R., Iimura, K., Wada, S., Shinjo, A., Benno, Y., Nakagawa, M., Takei, M., & Aida, Y. (2021). UVC disinfects SARS-CoV-2 by induction of viral genome damage without apparent effects on viral morphology and proteins. *Scientific Reports*, *11*(1), 1–11.

Loveday, E. K., Hain, K. S., Kochetkova, I., Hedges, J. F., Robison, A., Snyder, D. T., Brumfield, S. K., Young, M. J., Jutila, M. A., Chang, C. B., & Taylor, M. P. (2021). Effect of inactivation methods on SARS-CoV-2 virion protein and structure. *Viruses*, *13*(4), 562.

Möller, L., Schünadel, L., Nitsche, A., Schwebke, I., Hanisch, M., & Laue, M. (2015). Evaluation of virus inactivation by formaldehyde to enhance biosafety of diagnostic electron microscopy. *Viruses*, *7*(2), 666–679.

Nolte, E., Cremer, T., Gallo, R. C., & Margolis, L. B. (2016). Extracellular vesicles and viruses: Are they close relatives? *Proceedings of the National Academy of Sciences*, *113*(33), 9155–9161.

Nunez Lopez, Y. O., Casu, A., & Pratley, R. E. (2021). Investigation of extracellular vesicles from SARS-CoV-2 infected specimens: A safety perspective. *Frontiers in Immunology*, *12*, 1209.

Patterson, E. I., Prince, T., Anderson, E. R., Casas-Sanchez, A., Smith, S. L., Cansado-Utrilla, C., Solomon, T., Griffiths, M. J., Acosta-Serrano, Á., Turtle, L., & Hughes, G. L. (2020). Methods of inactivation of SARS-CoV-2 for downstream biological assays. *The Journal of Infectious Diseases*, *222*(9), 1462–1467.

Puray-Chavez, M., LaPak, K. M., Schrank, T. P., Elliott, J. L., Bhatt, D. P., Agajanian, M. J., Jasuja, R., Lawson, D. Q., Davis, K., Rothlauf, P. W., Liu, Z., Jo, H., Lee, N., Tenneti, K., Eschbach, J. E., Shema Mugisha, C., Cousins, E. M., Cloer, E. W., Vuong, H. R., … Kutluay, S. B. (2021). Systematic analysis of SARS-CoV-2 infection of an ACE2-negative human airway cell. *Scientific Reports*, *36*(2), 109364. https://doi.org/10.1016/j.celrep.2021.109364

Sanders, B., Koldijk, M., & Schuitemaker, H. (2015). Inactivated Viral Vaccines. In B. K. Nunnally, V. E. Turula, & R. D. Sitrin (Eds.), *Vaccine analysis: Strategies, principles, and control* (pp. 45–80). Springer Berlin Heidelberg.

Tey, S. K., Lam, H., Wong, S. W. K., Zhao, H., To, K. K., & Yam, J. W. P. (2022). ACE2-enriched extracellular vesicles enhance infectivity of live SARS-CoV-2 virus. *Journal of Extracellular Vesicles*, *11*(5), e12231. https://doi.org/10.1002/jev2.12231

Théry, C., Witwer, K. W., Aikawa, E., Alcaraz, M. J., Anderson, J. D., Andriantsitohaina, R., Antoniou, A., Arab, T., Archer, F., Atkin-Smith, G. K., Ayre, D. C., Bach, J. M., Bachurski, D., Baharvand, H., Balaj, L., Baldacchino, S., Bauer, N. N., Baxter, A. A., Bebawy, M., … Zuba-Surma, E. K. (2018). Minimal information for studies of extracellular vesicles 2018 (MISEV2018): A position statement of the International Society for Extracellular Vesicles and update of the MISEV2014 guidelines. *Journal of Extracellular Vesicles*, *7*(1), 1535750.

Welch, S. R., Davies, K. A., Buczkowski, H., Hettiarachchi, N., Green, N., Arnold, U., Jones, M., Hannah, M. J., Evans, R., Burton, C., Burton, J. E., Guiver, M., Cane, P. A., Woodford, N., Bruce, C. B., Roberts, A. D. G., & Killip, M. J. (2020). Analysis of inactivation of SARS-CoV-2 by specimen transport media, nucleic acid extraction reagents, detergents, and fixatives. *Journal of Clinical Microbiology*, *58*(11), e01713–01720.

Xie, H., Wang, Z., Zhang, L., Lei, Q., Zhao, A., Wang, H., Li, Q., Cao, Y., Jie Zhang, W., & Chen, Z. (2017). Extracellular vesicle-functionalized decalcified bone matrix scaffolds with enhanced pro-angiogenic and pro-bone regeneration activities. *Scientific Reports*, *7*(1), 1–13.

Yang, Q., Diamond, M. P., & Al-Hendy, A. (2016). The emerging role of extracellular vesicle-derived miRNAs: Implication in cancer progression and stem cell related diseases. *Journal of Clinical Epigenetics*, *2*(1), 13.

SUPPORTING INFORMATION

Additional supporting information can be found online in the Supporting Information section at the end of this article.

How to cite this article: Kongsomros, S., Pongsakul, N., Panachan, J., Khowawisetsut, L., Somkird, J., Sangma, C., Kanjanapruthipong, T., Wongtrakoongate, P., Chairoungdua, A., Pattanapanyasat, K., Newburg, D. S., Morrow, A. L., Hongeng, S., Thitithanyanont, A., & Chutipongtanate, S. (2022). Comparison of viral inactivation methods on the characteristics of extracellular vesicles from SARS-CoV-2 infected human lung epithelial cells. *Journal of Extracellular Vesicles*, *11,* e12291. https://doi.org/10.1002/jev2.12291